Aalborg Universitet

AALBORG UNIVERSITY
DENMARK

Energetic Cluster-Surface Interactions

Popok, Vladimir; Vuckovic, Sasa; Campbell, Eleanor E.B.; Jensen, Jens; Samela, Juha; Nordlund, Kai

Published in:
Proceedings of XIX International Conf. on Ion-Surface Interactions, Zvenigorod, Aug. 21-25 2009

Publication date:
2009

Document Version
Publisher's PDF, also known as Version of record

Link to publication from Aalborg University

Citation for published version (APA):
Popok, V., Vuckovic, S., Campbell, E. E. B., Jensen, J., Samela, J., & Nordlund, K. (2009). Energetic Cluster-Surface Interactions. In *Proceedings of XIX International Conf. on Ion-Surface Interactions, Zvenigorod, Aug. 21-25 2009* (Vol. 1, pp. 49-54).

General rights
Copyright and moral rights for the publications made accessible in the public portal are retained by the authors and/or other copyright owners and it is a condition of accessing publications that users recognise and abide by the legal requirements associated with these rights.

- Users may download and print one copy of any publication from the public portal for the purpose of private study or research.
- You may not further distribute the material or use it for any profit-making activity or commercial gain
- You may freely distribute the URL identifying the publication in the public portal -

Take down policy
If you believe that this document breaches copyright please contact us at vbn@aub.aau.dk providing details, and we will remove access to the work immediately and investigate your claim.

Downloaded from vbn.aau.dk on: April 18, 2024

ENERGETIC CLUSTER-SURFACE INTERACTIONS

V.N. Popok[1], S. Vučković[1], E.E.B. Campbell[1,2], J. Jensen[3], J. Samela[4] and K. Nordlund[4]

[1] *Department of Physics, University of Gothenburg, 41296 Gothenburg, Sweden, e-mail: popok@physics.gu.se*
[2] *School of Chemistry, Edinburgh University, EH9 3JJ Edinburgh, Scotland*
[3] *Department of Physics, Chemistry and Biology, Linköping University, 581 83 Linköping, Sweden*
[4] *Department of Physics, University of Helsinki, 00014 Espoo, Finland*

Atomic and molecular clusters are considered to be a distinct form of matter, a "bridge" connecting individual atoms on the one hand and solids on the other one. Interest in clusters comes from various fields. They can be used as models for investigation of fundamental physical aspects of the transition from atomic scale to bulk material as well as controllable and versatile tools for modification and processing of surfaces and shallow layers on the nanometer scale. However, practical applications of clusters require a good knowledge of the physics behind the interaction of energetic atomic agglomerates with matter which is fundamentally different from that of monomers [1-3].

Clusters generate multiple-collision effects during the penetration into the target that leads to the overlap of radiation cascades and causes high radiation damage. The interaction is also characterized by a high degree of nonlinearity, the cluster constituents influence each other during the penetration into the target. The stopping power of clusters in matter is reduced compared to monomers due to the so-called clearing-the-way effect, where the "front" atoms of the cluster push target atoms out of the way of the "rest" atoms [3, 4]. A violent interaction of the cluster with the surface layers of the target leads to extensive mixing of cluster constituents with substrate atoms that favours doping of very shallow layers for applications in electronics [2]. The effect of the high density of the energy transferred from the cluster at the beginning of impact in the case of high kinetic energy (velocity) can be compared with a meteorite-planet collision that typically results in crater formation. Thus, high-fluence energetic cluster beams can be used for efficient sputtering of surfaces and smoothing [2].

In this paper we will present our recent results on the interaction of keV-energy Ar_n clusters with silicon, rutile (TiO_2) and highly-ordered pyrolytic graphite (HOPG).

For the first series of experiments, Ar_n^+ cluster ions (with n from 11 to 55) having energies of 3-18 keV/cluster were implanted into both Si covered by a native oxide layer (SiO_2/Si) and sputtered (without the oxide layer) Si. To clarify the role of the substrate in the cluster-surface interaction, a few implantations of keV-energy Ar_n^+ cluster ions were also carried out

into HOPG. The implantations were performed using the cluster implantation and deposition apparatus together with the pulsed cluster source at room temperature in ultra-high vacuum of (1-2)×10^{-9} Torr [5, 6]. The experiments were complemented by classical molecular dynamics (MD) simulations. The interaction model for silicon that was used is based on the Stillinger-Weber potential and it is described in more detail in [7]. An improved Tersoff potential was used for the graphite simulations [8]. Argon clusters were described using a Lennard-Jones potential. For the second series of experiments, keV-energy Ar_n^+ cluster ions were implanted into rutile (TiO_2). The formation of surface defects generated by the clusters was compared to those formed after bombardment of MeV to GeV-energy multiply-charged I^{q+}, U^{q+} and Ta^{q+} ions with fluences of 10^9-10^{10} cm^{-2}.

The implanted surfaces were analysed by a scanning probe microscope Ntegra (NT-MDT) either using atomic force microscopy (AFM) in tapping mode or scanning tunnelling microscopy (STM) in constant current mode. Ultra sharp DLC cantilevers with a tip curvature radius of 1-3 nm were used for the AFM. Sharp tips of PtIr were used for the STM.

Impact of keV-energy clusters on SiO_2/Si samples typically results in crater formation. Along with craters, hillocks were found experimentally [6]. They typically have heights of a few nm and they are located inside craters forming so-called complex craters, i.e. a hillock surrounded by a rim [9]. A model of the hillock formation is based on the effect of multiple collisions causing a high density of energy deposition via the nuclear stopping mechanism resulting in a local melting of material around the impact spot. Local tensions and elastic rebound lead to viscous flow and expulsion of the molten material forming the hillock. However, the formation mechanism of the surrounding rim is uncertain because it typically varies between 20-50 nm in diameter for the used cluster energies and sizes [9]. These values are too large for the rim to be just material which is expulsed on the cluster impact. MD simulations predict crater diameters of just a few nm [7, 8]. Thus, some other origin for the formation of the surrounding rim should be considered.

Recent MD simulations of cluster collisions with Si demonstrated that the impact leads to the collective movement (oscillations) of the target atoms around the collision cascade on the ps time scale [7]. First, the atoms move downwards and away from the cascade. Then a counter movement occurs. Taking into account that the target material is locally molten, one can infer the existence of a surface wave propagating away from the impact spot. Quenching of this wave may lead to the rim formation. This process significantly depends on the composition of the layer where the cluster stops. Si wafers typically have a 2-3 nm thick oxide layer on the surface. MD simulations of Ar cluster impacts with energies of 3-15 keV show that lat-

eral velocities of the target atoms around the collision cascade have a maximum at the depth of ca. 2-3 nm, i.e. at the interface of SiO_2 and Si [7]. Since these materials have different properties, in particular, melting points, densities and thermal conductivities, the complex crater formation can be affected by the presence or absence of the SiO_2 layer.

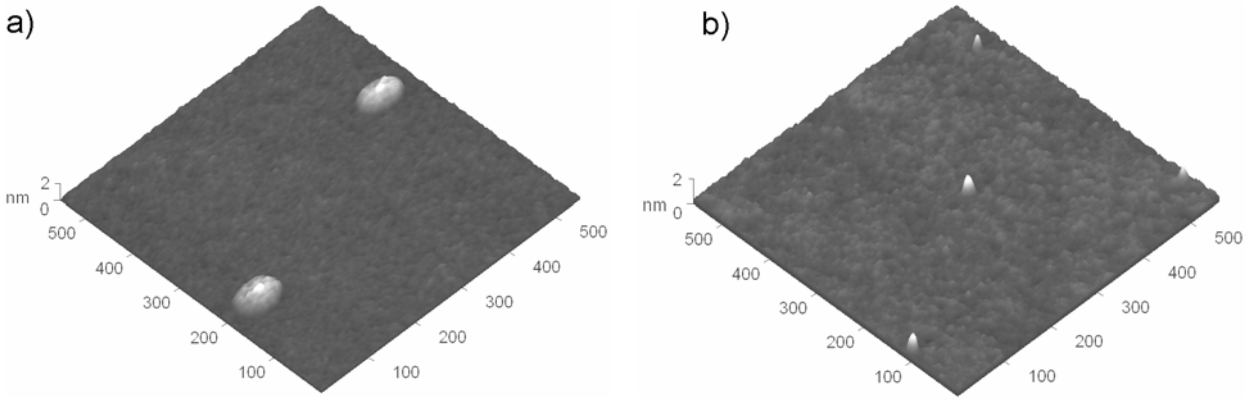

Fig. 1. AFM images of (a) unsputtered and (b) sputtered Si implanted by 15 keV Ar_{43} clusters.

To test this suggestion, Ar_n^+ cluster ion implantation was compared for non-sputtered (with the oxide layer) and sputtered (without the oxide layer) Si(111). An Ar ion gun with an energy of 1 keV was used for the sputtering. To eliminate the effect of amorphisation originated by sputtering, the samples were annealed *in situ* after the sputtering at T = 550 ^oC for 15 min.

The samples were implanted by 15 keV Ar_{43}^+ cluster ions. On the non-sputtered sample both complex and simple craters are found but the complex structures (Fig. 1a) are dominant, accounting for 60-70 %, while on the sputtered and annealed sample mainly hillocks (without surrounding rim) are observed (Fig. 1b). The hillocks found on the latter sample can represent simple craters with very narrow opening which is not resolved due to the AFM tip convolution [7]. These observations support the modelling data about the crucial role of thin layers and interfaces on the development of radiation cascades and the formation of nanostructures on shallow cluster implantation.

In the case of graphite, there were no craters found for cluster sizes up to ca. 40 atoms and implantation energies up to 17 keV/cluster. Instead, small bumps with height of 0.4-0.6 nm and diameter of 5-7 nm are seen by STM (Fig. 2a). The MD simulations show that graphite responds very elastically to cluster impact, the cluster collision induces oscillations of the lattice planes and a relatively large destroyed region of the graphite structure in the early phase of the collision can partly recover and the crater can be closed on the longer (few tens of ps) time scale [8]. Thus, the observed bumps are suggested to be highly-disordered impact areas and, if there is a small crater opening, it is not resolved by the STM tip.

It is known that oxidative etching of graphite at 600-650 ^oC can lead to the formation of pits at the spots where the defects are present. These pits are typically circular or hexagonal in

shape. The depth of the pits depends on the depth of the radiation damage cascades developed by the projectiles because the etching removes only the damaged graphite and it does not remove the graphite planes below the damaged volume [10]. Hence, one can estimate the radiation damage depth from the etching experiments. A series of these experiments varying the cluster size and impact energy is under progress. One of the AFM images corresponding to the case of 17 keV Ar_{41}^{+} cluster ion implantation is presented in Fig. 2b.

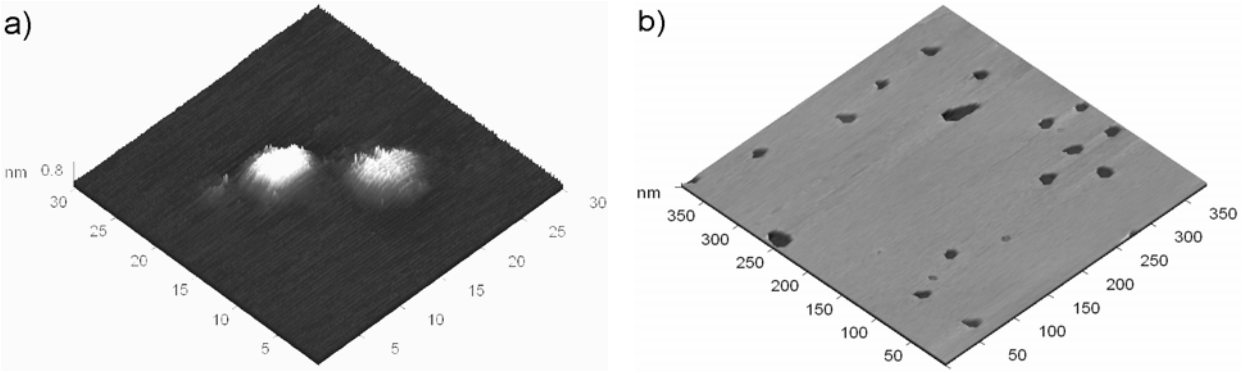

Fig. 2. STM images of HOPG (a) as-implanted by 15 keV Ar_{36} clusters and (b) implanted by17 keV Ar_{41} clusters and then oxidatively etched (the pits are 8±2 graphite planes deep).

For the case of rutile, the formation of simple craters with rim-to-rim diameter of 10-20 nm is observed on the cluster impact. There was no difference for the crater diameters found for different cluster energies. This leads us to the conclusion that there is no significant effect of the cluster energy change (for the used energy interval of 6.9-17.25 keV/cluster) on the lateral development of the radiation-damaged region. The crater formation can be explained by the multiple-collision effect leading to a high density of energy and high momentum transferred from the cluster to target atoms that leads to local compression, rapid heating and development of a shock wave. The impact region becomes strongly disordered and the atoms receive a high kinetic energy with a large fraction of them – those present in the edges of crater – obtaining momenta directed away from the surface.

Despite the significant difference in the stopping mechanisms for low-energy cluster ions and high-energy monoatomic multiply-charged ions, similar craters to the ones observed on cluster impact are found after implantation of 40 and 46 MeV I^{9+} and I^{10+} ions (Fig. 3a). Impact of a MeV highly-charged ion on rutile leads to a very fast transfer of a huge amount of energy in the very beginning of the track through electronic stopping. This transfer causes development of a thermal spike and in addition the Coulomb explosion effect that in turn can originate crater formation. This was predicted by MD simulations for Xe^{q+} ion implantation in Si [11] and it was found experimentally on TiO_2 surfaces bombarded by Xe^{q+} ions [12].

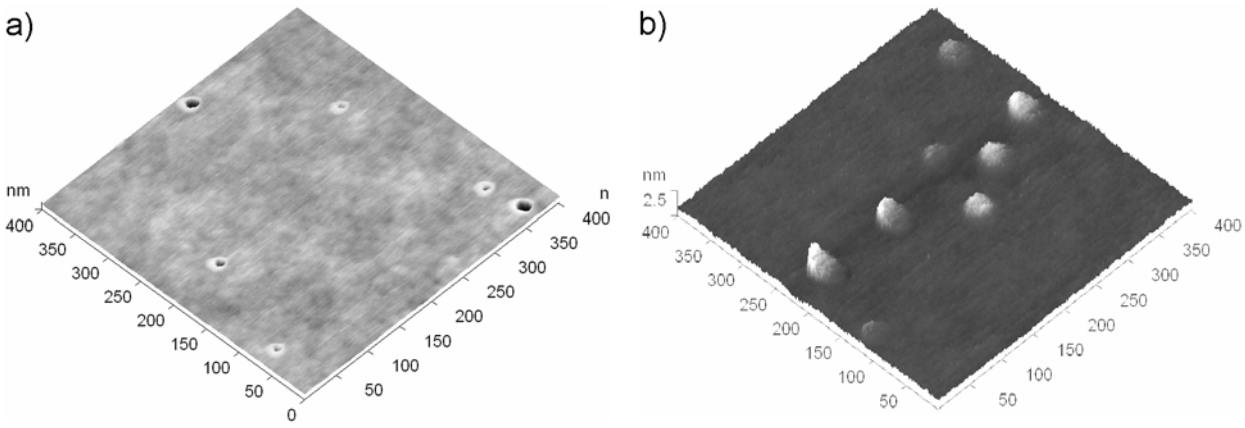

Fig. 3. AFM images of rutile implanted by (a) 40 MeV I^{9+} and (b) 1.2 GeV Ta^{q+} ions.

Contrary to the case of MeV implantation, bombardment by 1.2 GeV U^{q+} and Ta^{q+} ions leads to hillock formation (Fig. 3b). The hillocks diameters vary between 25-40 nm and the heights between 1-5 nm for both samples. Hillock formation under the implantation of swift heavy ions was previously observed on a number of materials [13-16]. The formation of nanosize protrusions was explained in terms of the thermal spike model, in which the energy is transferred through electronic stopping from the ion to the target atoms, leading to melting of the material surrounding the latent track. The molten phase is pushed out and quenched, thus forming the hillock. The electronic stopping power S_e is one of the critical parameters. At high enough S_e, a continuous cylindrical track can be formed. The radius of the track increases with S_e and at certain values of radius (≥ 3nm), the damage in the track becomes homogeneous. This is one of the necessary conditions for the track appearance on the surface [16]. It was recently shown elsewhere [17] that for iodine ion implantation into rutile, the energy of 120 MeV just slightly overcomes the threshold for the formation of continuous tracks, i.e. the energy is enough for the melting of material along the whole track. The corresponding S_e value is found to be 21.5 keV/nm according to SRIM2003 [18]. Simulations for our energies of 40 and 46 MeV give values of ca. 13 and 14 keV/nm, correspondingly. Thus, the S_e values in our case are significantly lower and the energy transferred from the ion to the target is probably not enough to cause formation of continuous tracks for which the temperature overcomes the melting point (2130 K). On the other hand, the electronic stopping powers for the case of 1.2 GeV implantations of tantalum and uranium are ca. 33 and 47 keV/nm, i.e. the threshold for the continuous track formation with molten phase can be overcome leading to the appearance of hillocks.

Hence, the crater formation on impact of MeV ions is related to the case when no continuous tracks are formed and the temperature along the whole track does not overcome the melting point. In this case, Coulomb explosion of the surface region is dominant due to the high

charge of the ions. The formation of hillocks on implantation of GeV ions is caused by the development of continuous tracks in which the material is molten. Elastic rebound due to tension between the molten and solid state phases leads to liquid flow, expansion and quenching effects.

1. V.N. Popok and E.E.B. Campbell, Rev. Adv. Mater. Sci. 11, (2006) 19.
2. N. Toyoda and I. Yamada, IEEE Trans. Plasma Sci. 36 (2008) 1471.
3. P. Sigmund, I. S. Bitensky, J. Jensen, Nucl. Instr. Meth. B 112 (1996) 1.
4. Y. Yamamura and T. Muramoto, Nucl. Instr. Meth. B 72 (1992) 331.
5. V.N. Popok, S.V. Prasalovich, M. Samuelsson, E.E.B. Campbell, Rev. Sci. Instr. 73 (2002) 4283.
6. V.N. Popok, S.V. Prasalovich, E.E.B. Campbell, Nucl. Instr. Meth. B. 207 (2003) 145.
7. J. Samela, K. Nordlund, V.N. Popok, E.E.B. Campbell, Phys. Rev. B 77 (2008) 075309.
8. J. Samela, K. Nordlund, J. Keinonen, V.N. Popok, and E.E.B. Campbell, Eur. Phys. J. D 43 (2007) 181.
9. S. Prasalovich, V.N. Popok, P.Persson, E.E.B. Campbell, Eur. Phys. J. D 36 (2005) 79.
10. G. Bräuchle, S. Richard-Scheider, D. Illig, R.D. Beck, H. Schreiber, M.M. Kappes, Nucl. Instr. Meth. B 112 (1996) 105.
11. Z. Insepov, P. Allain, A. Hassanein, M. Terasawa. Nucl. Instr. Meth. B 242 (2006) 498.
12. M. Tona, H. Watanabe, S. Takahashi, Y. Fujita, T. Abe, S. Jian, N. Nakamura, N. Yoshiyasu, C. Yamada, M. Sakurai, S. Ohtani. J. Phys.: Conf. Ser. 58 (2007) 331.
13. A.S. El-Said, R. Neumann, K. Schwartz, C. Trautmann. Surf. Coat. Technol. 158-159 (2002) 522.
14. A.S. El-Said, M. Cranney, N. Ishikawa, A. Iwase, R. Neumann, K. Schwartz, M. Toulemonde, C. Trautmann. Nucl. Instr. Meth. B 218 (2004) 492.
15. M. Lang, U.A. Glasmacher, B. Moine, C. Muller, R. Neumann, G.A. Wagner. Surf. Coat. Technol. 158-159 (2002) 439.
16. M. Toulemonde, C. Trautmann, E. Balanzat, K. Hjort, A. Weidinger. Nucl. Instr. Meth. B 216 (2004) 1.
17. K. Awazu, X. Wang, M. Fujimaki, T. Komatsubara, T. Ikeda, Y. Ohki. J. Appl. Phys. 100 (2006) 044308.
18. www.srim.org